Eur. Phys. J. C (2026) 86:58
https://doi.org/10.1140/epjc/s10052-025-15252-0

THE EUROPEAN PHYSICAL JOURNAL C

Regular Article - Theoretical Physics

Energetics of accretion disk around black holes in Einstein–Gauss–Bonnet gravity

Ikrom Ergashov[1,a], **Bakhtiyor Narzilloev**[1,b], **Ibrar Hussain**[2,7,c], **Ahmadjon Abdujabbarov**[3,4,5,d], **Bobomurat Ahmedov**[1,3,6,e]

[1] Institute for Advanced Studies, New Uzbekistan University, Movarounnahr Str. 1, 100000 Tashkent, Uzbekistan
[2] School of Electrical Engineering and Computer Science, National University of Sciences and Technology, H-12, Islamabad, Pakistan
[3] School of Physics, Harbin Institute of Technology, Harbin 150001, People's Republic of China
[4] Tashkent State Technical University, 100095 Tashkent, Uzbekistan
[5] Institute of Nuclear Physics, Ulugbek 1, 100214 Tashkent, Uzbekistan
[6] Institute of Theoretical Physics, National University of Uzbekistan, 100174 Tashkent, Uzbekistan
[7] Research Center of Astrophysics and Cosmology, Khazar University, 41 Mehseti Street, AZ1096 Baku, Azerbaijan

Received: 20 October 2025 / Accepted: 20 December 2025

Abstract We investigate the spacetime geometry and astrophysical properties of a static, spherically symmetric black hole in the context of Einstein–Gauss–Bonnet gravity, characterized by a Gauss–Bonnet coupling constant κ and a non-electromagnetic geometric charge Q. The black hole solution reduces to the Reissner–Nordstrom or Schwarzschild spacetime in the appropriate limits. We analyze the influence of the parameters κ and Q on the event horizon properties, the innermost stable circular orbit, and the spacetime metric behavior. In the framework of the Novikov–Thorne thin disk model, we compute the flux, temperature, and spectrum of the accretion disk surrounding the black hole. Our results show that the parameters κ and Q significantly affect the disk's thermal properties and radiation efficiency. Additionally, we demonstrate that the combined effect of these parameters can mimic the role of spin in Kerr black holes, allowing for degeneracy between rotation and geometric corrections. These findings offer potential observational signatures of modified gravity effects in high-energy astrophysical environments.

1 Introduction

Black holes, among the most intriguing predictions of General Relativity (GR), serve as natural laboratories for probing the fundamental nature of gravity under extreme conditions. GR predicted remarkable phenomena such as gravitational waves and black hole shadows, which have now been confirmed by observations [1,2]. In recent years, interest in modified or alternative theories of gravity has grown substantially, motivated by efforts to reconcile GR with quantum field theory and to explain cosmological phenomena such as dark energy, which is believed to be responsible for the accelerated expansion of the Universe [3,4]. Among the modifications of GR, Einstein–Gauss–Bonnet (EGB) gravity [5] has attracted significant attention, as it introduces higher-curvature corrections to the Einstein–Hilbert action through the Gauss–Bonnet (GB) term, parameterized by a coupling constant κ. The GB term was first introduced by Lanczos [5] in the context of four-dimensional gravity, where it appears as a topological invariant and does not contribute to the field equations. Later, Lovelock [6,7] systematically derived the most general second-order field equations for a metric theory of gravity in arbitrary dimensions. This theory does not introduce extra fundamental fields and naturally avoids Ostrogradsky instabilities [8]. In this framework, the GB term arises as the second-order contribution in what is now known as the Lovelock series. For $D < 5$ dimensions, the GB term does not affect the dynamics. However, Glavan and Lin [9] proposed a rescaling of the coupling constant to circumvent the Lovelock theorem and obtain non-trivial four-dimensional

[a] e-mail: i.ergashov@newuu.uz
[b] e-mail: b.narzilloev@newuu.uz
[c] e-mail: ibrar.hussain@seecs.nust.edu.pk (corresponding author)
[d] e-mail: ahmadjon@astrin.uz
[e] e-mail: ahmedov@astrin.uz

Published online: 22 January 2026

dynamics. In this context, black hole solutions in EGB gravity exhibit intriguing deviations from their general relativistic counterparts [10].

Black holes, both in GR and in modified theories of gravity, have attracted significant attention from researchers in various contexts [11–18]. Static and rotating black hole solutions in four-dimensional EGB gravity have been derived in the literature [19,20]. Various physical phenomena in the vicinity of black holes, including particle dynamics and associated effects such as gravitational lensing, black hole shadows, quasi-periodic oscillations, quasinormal modes, and thermodynamics, have been investigated [21–25]. The different characteristics of certain black hole solutions have also been analyzed in our earlier studies [26–34].

Accretion discs, which are responsible for the mass accumulation of black holes [35], are considered highly significant in the field of black hole astrophysics. As matter spirals toward the event horizon, electromagnetic radiation is emitted across a broad spectrum, from X-rays to radio waves due to the intense friction and compressional heating. This radiation enables the detection and study of black holes that would otherwise remain hidden. The efficiency with which energy is released during the accretion process plays a key role in the evolution of black holes (see, e.g., [36]). Accretion processes also power some of the most energetic astrophysical phenomena in the Universe, including quasars and active galactic nuclei (AGN), allowing entire galaxies to be observed over immense cosmic distances.

Accreting black holes frequently launch powerful relativistic jets that can transport energy and matter far beyond their host galaxies [37]. These jets interact with the interstellar and intergalactic medium, influencing star formation and shaping the large-scale structure and evolutionary pathways of galaxies through a mechanism known as AGN feedback [38]. The regions where accretion and jet formation occur, where gravitational fields and relativistic effects are extremely strong, serve as ideal laboratories for testing the theory of GR and alternative theories of gravity, including the EGB gravity [39]. Despite decades of investigation, the precise mechanisms behind jet launching, collimation, and acceleration, particularly those involving magnetic field interactions and frame-dragging effects, remain only partially understood. Continued exploration of these phenomena holds the promise of advancing our understanding of black hole spin dynamics, magnetohydrodynamics and the behavior of matter under extreme physical conditions.

In this work, we focus on a static, spherically symmetric black hole in the EGB gravity characterized by two key parameters, the GB coupling constant κ and a non-electromagnetic geometric charge Q. This geometric charge differs from the standard Maxwell charge and arises purely from spacetime geometry, allowing the black hole solution to interpolate between Schwarzschild and Reissner–Nordström limits in the appropriate regimes [40]. By systematically analyzing the dependence of the metric structure on κ and Q, we identify how these parameters influence essential black hole features such as the event horizon radius and the innermost stable circular orbit (ISCO). These quantities are of central importance in astrophysics, as they directly determine the motion of matter and the structure of accretion flows around black holes [41].

To explore the astrophysical implications of these geometric modifications, we employ the Novikov–Thorne thin disk model [42], a well-established framework for describing steady-state, optically thick, geometrically thin accretion disks. Within this formalism, we compute the energy flux, temperature distribution, and emission spectrum of matter accreting onto the EGB black hole. Our results reveal that both κ and Q play a crucial role in shaping the thermal and radiative properties of the disk. Specifically, variations in these parameters can lead to significant shifts in peak emission frequency, total radiative efficiency, and the overall spectral shape, offering potential observational signatures that could distinguish EGB black holes from their general relativistic analogs. Interestingly, we find that the combined influence of κ and Q can mimic the effects of black hole spin in the Kerr metric. This degeneracy between rotation and geometric corrections presents both a challenge and an opportunity, while it complicates the interpretation of observational data, it also opens the possibility of constraining modified gravity effects using high-resolution measurements of accretion disks, such as those obtained from X-ray spectroscopy or the Event Horizon Telescope [42]. The results of this study highlight the importance of considering beyond the GR parameters in black hole astrophysics and demonstrate that EGB gravity offers a rich phenomenology with potentially measurable consequences in high-energy cosmic environments.

We organize our work as follows. In the next section, the spacetime geometry of the EGB gravity black hole is described. In Sect. 3, the Novikov–Thorne disk model for the black hole accretion is discussed. Section 4 is devoted to the thermal properties of the accretion disk. In the last section, a conclusion and discussion of the work is presented.

2 Spacetime geometry of the black hole

The action of EGB gravity in D-dimensional spacetime is

$$S_0 = \frac{1}{16\pi}\int d^D x\sqrt{-g}\left[2\Lambda + R + \alpha\mathcal{G} - F_{\mu\nu}F^{\mu\nu}\right] + S_{\text{matter}}. \tag{1}$$

Here, Λ stands for the cosmological constant, and the Ricci scalar R is the Einstein–Hilbert term. The Gauss–Bonnet term $\mathcal{G}$ is scaled by a coupling constant α and the Gauss–

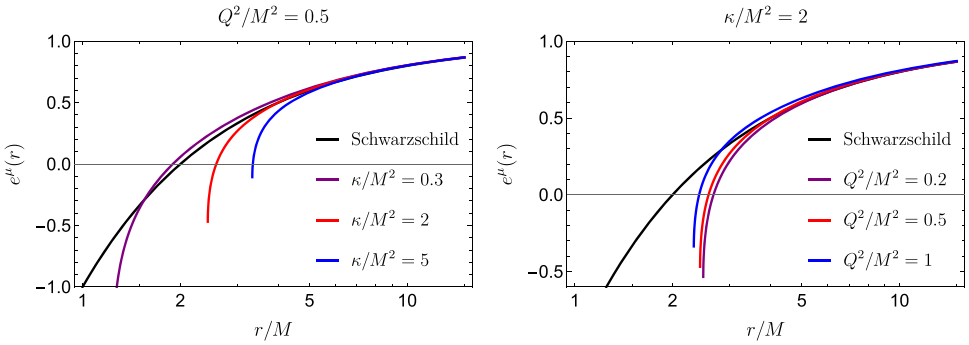

Fig. 1 The dependence of metric function on normalized radial coordinate for different parameter values. The right side graph shows the fixed Q^2/M^2, while a graph on left indicates the fixed κ^2/M^2

Bonnet term can be defined $\mathcal{G} = R_{\mu\nu\rho\sigma}R^{\mu\nu\rho\sigma} - 4R_{\mu\nu}R^{\mu\nu} + R^2$. Additional terms S_{matter} and $F_{\mu\nu}$ represent the action of any additional fields and the electromagnetic field tensor, respectively. In Ref. [43], the author focuses on deriving solutions to the field equations within degenerate Einstein—Gauss–Bonnet (dEGB) gravity, which is constructed using degenerate vielbeins such that the extra dimensions have zero proper length. This construction yields a four-dimensional theory that is purely metric-based, generally covariant, and free from Ostrogradsky instabilities.

The solution is considered as a static, spherically symmetric spacetime metric with the lapse function:

$$e^{\mu} = 1 - \frac{r^2}{2\kappa}\left[1 - \left(1 - \frac{8M\kappa}{r^3} + \frac{4Q^2\kappa}{r^4}\right)^{\frac{1}{2}}\right] \tag{2}$$

with $\left|\frac{\alpha}{\phi}\right| = \kappa > 0$. This is the metric form that will be used in subsequent calculations involving the positive branch, with non-zero parameters Q and κ. The Gauss–Bonnet parameter κ expresses its influence on gravitational fields. If we take the limit κ to zero ($\kappa \to 0$) for this spacetime, we get exactly the Reissner–Nordstrom spacetime. Also, by obtaining the disappearance of the geometric charge ($Q = 0$), both of these conditions can provide the standard Schwarzschild metric.

However, in our spacetime, Q is not the same as the charge that came from Maxwell Electrodynamics. Instead, it is a geometric charge that is built into the structure of spacetime itself. Unlike electric charge, Q does not relate to particles or fields. It emerges completely from the geometry of the theory. It appears in the equations similarly to ordinary charge but modifies gravity in a new way. There are no local sources that carry this geometric charge by particle or field, and it is purely source-free. It only arises from the geometric structure of spacetime and has been derived and investigated in [44].

Firstly, in this study, we focus on the influences of both κ and Q parameters of the black hole on the spacetime properties. Therefore, we would like to illustrate the behavior of the normalized radial coordinate-dependent metric function for the black hole with fixed coupling constant κ and fixed geometric charge Q.

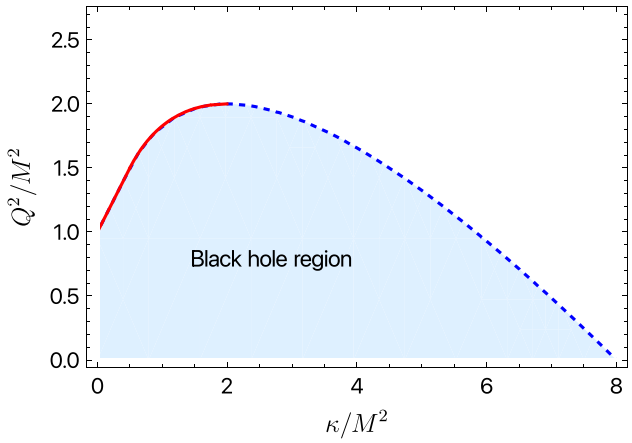

Fig. 2 Blue region: where the outer event horizon exists. Red lines: reach the highest radiation efficiency of the black hole

As we expected, the metric function Eq. (2) tends towards 1, when we investigate the larger coordinate values as indicated in Fig. 1. One can conclude that the metric components $g_{\mu\nu}$ are to be considered as those of the Minkowski metric at large distances from the origin (matter or energy concentration) due to the diminishing influence of the gravitational source, which suggests that the metric can satisfy the necessary condition for asymptotic flatness at infinity. However, the results of parameters κ and geometric charge Q in Fig. 1 show that at near distances, the parameters significantly affect, especially the contribution of κ, compared to geometric charge Q, which is much higher. In particular, the charge Q can significantly affect our spacetime, when we work with small values of the κ parameters.

One of the parameters of the black hole that we need to know is the event horizon radius. The values of the radius of the event horizon of the EGB black hole, we consider here, lie at the roots of $e^{\mu} = 0$, and they are located at

$$r_{\pm} = M\left(1 \pm \sqrt{1 - \frac{Q^2}{M^2} + \frac{\kappa}{M^2}}\right), \tag{3}$$

r_+ and r_- are the outer and inner event horizons. It is obvious that the inner event horizon disappears when we consider a

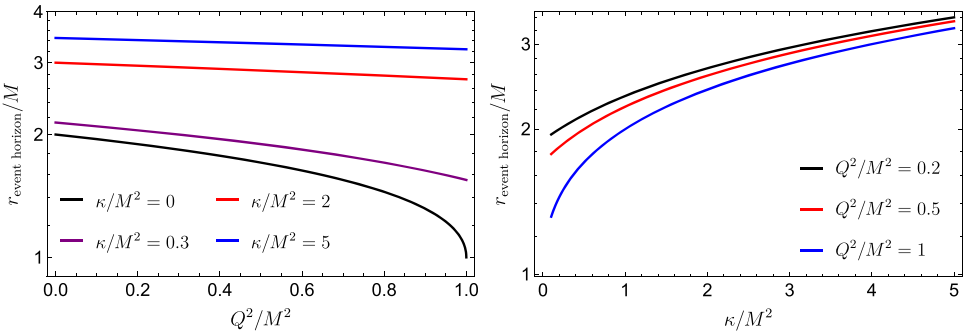

Fig. 3 Horizon radius dependence on different parameters

higher value of Q and κ. Therefore, we are only interested in the outer event horizon.

We determined the range of metric parameters κ and Q^2 where our event horizon exists, as can be seen from Fig. 2 while naked singularities arise from these parameter values indicated by the blue dashed and red lines on the graph. Notice that the red lines not only indicate the region of naked singularity but also the specific thin parameter region close to this line, which shows up as a result is the highest radiation efficiency; this will be explored further in the subsequent work.

In Fig. 3, the dependence of the black hole event horizon radius on the parameters κ and Q is shown. The figure indicates that increasing the value of Q, due to its interaction with the charged matter of the accretion disk, leads to a shrinking of the event horizon radius. In contrast, the outer horizon increases when κ is increased simultaneously, showing that the influence of Q becomes less dominant for larger values of κ. This leads us to conclude that the outer event horizon attains its maximum value when $Q = 0$ and κ reaches its maximum, i.e., $\kappa/M^2 = 8$ (yielding $r_+^{\max}/M = 4$). Conversely, the minimum value of the outer event horizon is $r_+^{\min}/M = 1$, which occurs when the discriminant under the square root in Eq. (3) vanishes.

Increasing the charge Q leads to a shrinking of the black hole horizon due to its interaction effects, and this influence becomes predominant as Q approaches its maximum value. This can be attributed to the stronger repulsive effect at large Q. The event horizon reaches its minimum possible size just before the black hole turns into a naked singularity. For small values of the parameter κ, the event horizon behaves consistently with the properties of the Reissner–Nordström metric. However, for larger κ, the horizon radius increases, weakening the influence of both charge and mass and allowing the event horizon to grow.

3 Novikov–Thorne model of the accretion disk

Here, we focus on the properties of an accretion disk that surrounds a black hole in a ring-like shape. We adopt the geometrically thin and optically thick Novikov–Thorne disk model, which generalizes the Shakura–Sunyaev approach [42]. In this model, the vertical size of the disk (the height from the equatorial symmetry plane, h) is negligible compared to its radial size (the distance from the center, r), i.e., $h \ll r$ at every point of the disk. This assumption allows us to neglect the effects of the disk's mass and charge on the surrounding spacetime. Additionally, the radial pressure and velocity gradients are assumed to be negligible in the emitting region. The accretion disk consists of high-temperature, high-pressure matter that steadily flows inward as hot gas and eventually falls onto the black hole. We further assume that the rate of matter flow remains constant over time, a quantity measured by the accretion rate, denoted by $\dot{M}$.

Another theoretically and practically important parameter is ISCO of particles around black holes, which is essential for investigating accretion disks and determining their inner edge. To derive the ISCO radius, we first write the radial equation of motion for matter particles in the equatorial plane ($\theta = \pi/2$), given as follows:

$$\left(\frac{dr}{d\tau}\right)^2 = E - V_{eff}, \tag{4}$$

where V_{eff} is the effective potential. There are two conserved quantities for each particle in accretion disks, one is its specific energy (the energy per unit mass) $E = -g_{tt}\dot{t} - g_{t\phi}\dot{\phi}$, and another one is the specific angular momentum (the angular momentum per unit mass) $L = g_{\phi t}\dot{t} + g_{\phi\phi}\dot{\phi}$.

Thus, the canonical effective potential of the accretion disk matter particles is represented in terms of the black hole parameters and by specific energy and specific angular momentum:

$$\begin{aligned} V_{\text{eff}}(r) &= -1 + \frac{E^2 g_{\phi\phi} + L^2 g_{tt} + 2EL g_{t\phi}}{g_{tt} g_{\phi\phi} - g_{t\phi}^2} \\ &= \frac{2\kappa\left(L^2 - \left(E^2+1\right) r^2\right) - Cr^2(L^2 - r^2)}{r^2(2\kappa - r^2 C)}. \end{aligned} \tag{5}$$

The specific energy E and the specific angular momentum L can be expressed with the components of the metric tensor as

$$E = -\frac{-g_{tt} - \Omega g_{\phi t}}{\sqrt{-g_{tt} - 2\Omega g_{t\phi} - \Omega^2 g_{\phi\phi}}} = \frac{2\kappa - r^2 C}{2\kappa\sqrt{2Q^2 - 3Mr + 1}} \quad (6)$$

and

$$L = -\frac{g_{tt}\Omega + g_{\phi t}}{\sqrt{-g_{tt} - 2\Omega g_{t\phi} - \Omega^2 g_{\phi\phi}}} = \sqrt{\frac{r^4 C - 2\kappa r M}{2\kappa C(2Q^2 - 3Mr + 1)}}. \quad (7)$$

The angular velocity of a particle in an equatorial circular orbit is given as:

$$\Omega = \frac{d\phi}{dt} = -\frac{-\partial_r g_{t\phi} + \sqrt{(\partial_r g_{tt})^2 - \partial_r g_{\phi\phi}\partial_r g_{tt}}}{\partial_r g_{\phi\phi}} = \sqrt{\frac{r^3 C - 2\kappa M}{2\kappa r^3(1 - C)}}, \quad (8)$$

where,

$$C = C(r, Q^2, \kappa) = 1 - \sqrt{\frac{-8\kappa M r + 4\kappa Q^2 + r^4}{r^4}}. \quad (9)$$

This is the full general form in terms of $g_{\mu\nu}$. It should be noted that if the particles have equatorial circular orbits on accretion disks, they must follow these conditions:

$$V_{\text{eff}}(r) = E, \qquad V'_{\text{eff}}(r) = 0. \quad (10)$$

The marginally stable orbit's radius (commonly referred to as ISCO) is defined as follows (together with the above equations):

$$V''_{\text{eff}}(r_{\text{isco}}) = 0. \quad (11)$$

Similarly, the ISCO radii are predicted to behave in the same way as the event horizon of this black hole with respect to variations in the charge Q and parameter κ, as shown in Fig. 4. Our calculations indicate that the ISCO radius can reach up to $R_{isco} = 8.62M$, which is significantly larger than the Schwarzschild ISCO radius ($6M$). The orbits become more stable at larger distances when the geometric charge vanishes ($Q = 0$) and κ attains its maximum value $\kappa/M^2 = 8$. Conversely, the ISCO radius approaches its minimum value near the event horizon, $r_{isco}^{\min} \approx r_{+}^{\min} = M$, when the discriminant under the square root vanishes ($Q = 1$), as shown in Eq. (3) and represented in the right panel of Fig. 4 by the blue solid line.

The results presented above suggests that the parameters κ and Q can mimic the spin parameter a of the Kerr black hole. It is well known that the spin parameter a of the Kerr black hole strongly affects the ISCO radius, specifically, an increase in a allows stable orbits to occur closer to the event horizon. Figure 5 shows the degeneracy lines (solid curves correspond to the black hole region) where the radius of the innermost stable circular orbit (r_{ISCO}) of the modified black hole coincides with that of the Kerr black hole with spin parameter a/M. The dashed curves indicate parameter regions in which no black hole horizon exists. These results show that the combined effects of κ and Q can mimic the behavior of the Kerr spin parameter up to $a/M \approx 0.866$, corresponding to the uncharged case.

4 Thermal properties

One of the ways to investigate the black hole is the behavior of the flux that emits electromagnetic radiation from the accretion disk, which can be observed to compare the difference between experimental results and theoretical calculations.

We assume particles move in circular geodesics in the equatorial plane. The following equation represents the flux of electromagnetic radiation:

$$F(r) = -\frac{\dot{M}_0}{4\pi\sqrt{-g}M^2}\frac{\Omega_{,r}}{(E - \Omega L)^2}\int_{r_{\text{isco}}}^{r}(E - \Omega L)L_{,r}dr. \quad (12)$$

The determinant of the black hole metric is denoted by g and we choose mass accretion rate $\dot{M}_0$ as a half of the Eddington accretion rate for a black hole of 10 solar masses.

The flux equation is too complex to be solved analytically for our modified gravity model with parameters κ and Q. Therefore, to compute the flux profile, we solve it numerically. We can then illustrate how the flux from the black hole depends on the distance by fixing the parameters κ and Q, as shown in Fig. 6.

The top panels show that the flux increases with larger values of Q, while the distance at which the flux reaches its peak decreases. This effect arises from the interaction between matter and the black hole. A higher charge allows stable orbits closer to the horizon, which in turn enlarges the emission region. In contrast, the effect of κ is opposite to that of Q, increasing κ reduces the flux, and the corresponding peak shifts outward.

The figures also reveal that near the ISCO radius, the flux rises sharply due to the presence of stable orbits. This effect is especially pronounced for smaller κ, leading to a steeper profile until the flux peak, after which it decreases asymptotically as matter becomes more diffuse. Beyond approximately $20M$, all flux profiles converge and become nearly indistinguishable. The radiation efficiency of the black hole measures the proportion of infalling matter's energy that is transformed into radiation (as light, heat, etc.) as it approaches the black hole before being accreted. The efficiency is calculated using

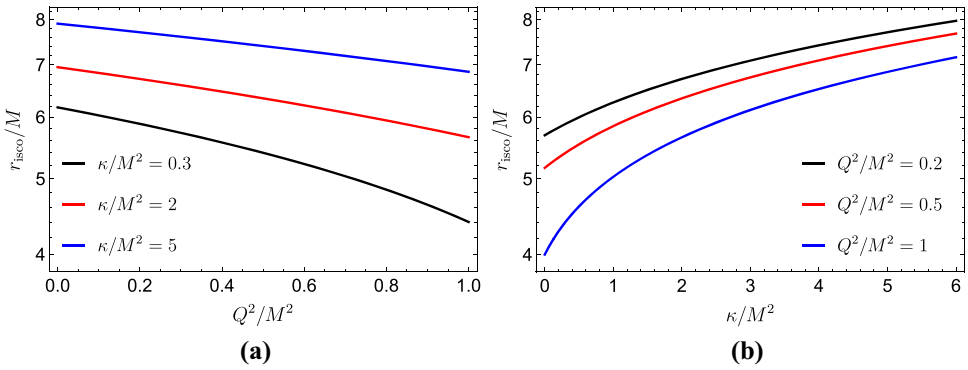

Fig. 4 ISCOs for different parameter configurations. **a** Variation with κ/M^2 shows. **b** The Q^2/M^2 dependence

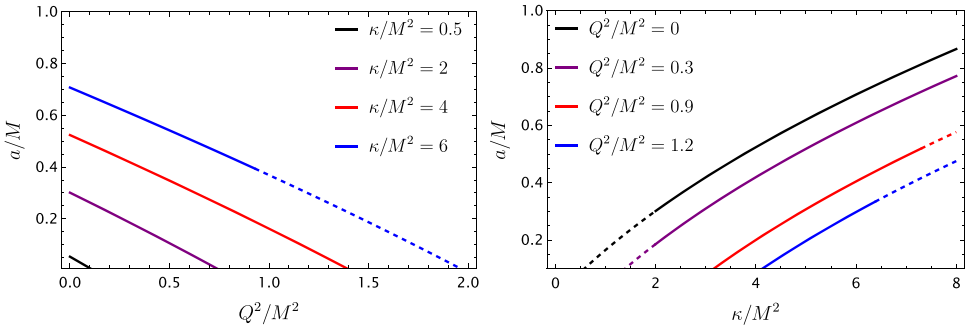

Fig. 5 Solid lines: Degeneracy plots illustrating the relationship between the dimensionless spin parameter a of the Kerr metric and the parameters Q and κ for fixed parameters. Dashed lines: No black hole region

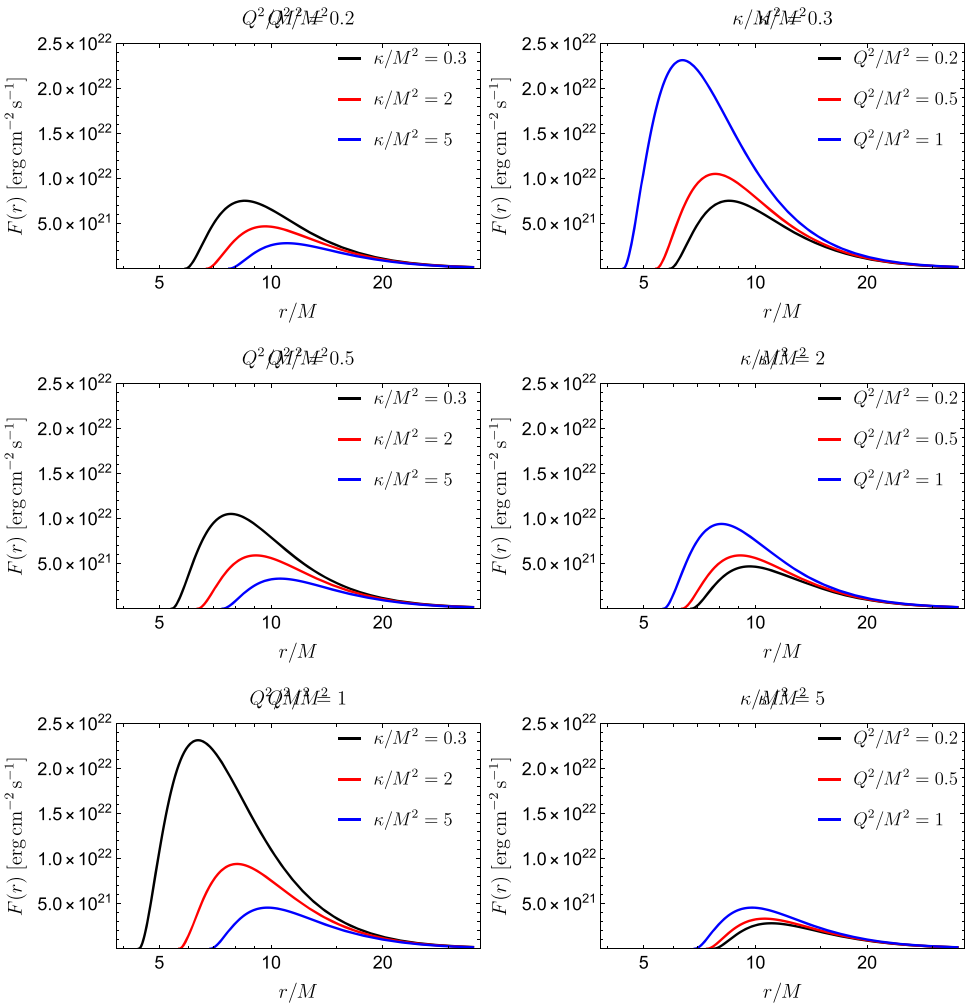

Fig. 6 Dependence of the flux of electromagnetic radiation of the disk on the radial coordinate for various values of the black hole parameters

Table 1 ISCO radius r_{isco} and radiation efficiency η for varying κ/M^2 and Q^2/M^2

Q^2/M^2	$\kappa/M^2 \to 0$		$\kappa/M^2 = 1$		$\kappa/M^2 = 2$		$\kappa/M^2 = 3$		$\kappa/M^2 = 4$		$\kappa/M^2 = 5$		$\kappa/M^2 = 6$	
	r_{isco}	η	r_{isco}	η	r_{isco}	η	r_{isco}	η	r_{isco}	η	r_{isco}	η	r_{isco}	η
0.0	6.000	5.719	6.530	5.359	6.953	5.097	7.311	4.891	7.626	4.723	7.908	4.580	8.164	4.457
0.2	5.688	6.004	6.267	5.574	6.716	5.273	7.092	5.042	7.418	4.856	7.710	4.700	7.974	4.566
0.4	5.349	6.346	5.990	5.820	6.470	5.470	6.865	5.209	7.205	5.001	7.506	4.829	7.779	4.684
0.6	4.972	6.773	5.695	6.106	6.212	5.693	6.629	5.394	6.985	5.161	7.297	4.971	7.578	4.811
0.8	4.538	7.333	5.378	6.447	5.941	5.948	6.384	5.601	6.757	5.337	7.082	5.125	7.373	4.949
1.0	4.000	8.144	5.034	6.864	5.655	6.244	6.128	5.836	6.520	5.534	6.860	5.295	7.161	5.100

this formula:

$$\eta = 1 - E_{\text{isco}} \tag{13}$$

where E_{isco} represents the energy of a particle at the ISCO.

Tables 1 and Fig. 7 provide the dependence of the radiation efficiency η on κ (for fixed Q) and on Q (for fixed κ). These plots reveal that increasing the geometric charge Q leads to higher efficiency values. This occurs because if Q increases, ISCO inclines more closely to the black hole's smaller orbit, meaning particles accelerate and also cause more fractional matter to lose its energy. By contrast, increasing the parameter κ produces the opposite effect, reducing the radiation efficiency. These behaviors and calculations indicate that radiation efficiency reaches its lowest point, at 4.25%, when $\kappa = 0$ and the geometric charge is zero. It achieves its peak value, close to the red line on Fig. 2 (where $1 < Q^2/M^2 < 2$ and $0 < \kappa/M^2 < 2$), when κ approaches its maximum and Q approaches its minimum, with an average maximum near 8.88%.

It is often assumed that the black hole's disk maintains thermal equilibrium, allowing us to apply the Stefan-Boltzmann law to determine the disk's temperature.

$$T(r) = \left(\frac{F(r)}{\sigma}\right)^{1/4}, \tag{14}$$

with Boltzmann constant σ. We know that black holes themselves cannot directly emit radiation, including light or X-rays. However, the infalling matter in the accretion disk undergoes strong dynamical friction and compression, leading to extremely high temperatures and, consequently, very bright luminosity. Accordingly, we obtain graphs for the black hole temperature that are identical in shape to those for the flux, as shown in Fig. 6. This is consistent with Eq. (14), which relates the flux to the fourth power of the temperature.

We have employed various fixed parameters to characterize the temperature profiles as density distributions. These profiles, shown in Figs. 8 and 9, arise from the flux dependence on the black hole parameters, and therefore exhibit the same qualitative behavior as the flux. In both figures, the purple regions correspond to the inner edge of the accretion disk (the ISCO radius), while the dark regions represent the interior of the event horizon. Additionally, the temperature increases with distance outward from the event horizon, reaching a peak of several million Kelvin. Beyond this peak, the influence of the parameters diminishes with increasing distance, so the green regions correspond to lower temperatures.

In Fig. 8, the temperature profiles are shown as 2D density plots across normalized positions $(X/M, Y/M)$, with T scaled from 0 to 4×10^6 (purple to red indicating increasing temperature). Each plot corresponds to different values of κ/M^2 and Q^2/M^2, highlighting their influence on the temperature distribution. For higher values of Q, the ISCO radius decreases, leading to higher temperatures. Conversely, increasing κ enlarges the ISCO radius, which reduces the temperature.

Alternatively, Fig. 9 presents the temperature profiles as density plots in terms of radial distance r and temperature T, using the same 0 to 4×10^6 scale. The color gradient illustrates how κ and Q affect the extent and intensity of the thermal halo, the central black region (lowest T) transitions outward into higher-temperature zones. At higher temperatures, the event horizon and the surrounding thermal gradient appear smaller as the ISCO radius shifts.

It can be assumed as blackbody radiation to obtain the luminosity of a thin accretion disk. The luminosity emanating from an accretion disk with inner and outer radii is r_{in} and r_{ex}, respectively, and has i as an inclination angle of the accretion disk, calculated as follows:

$$L(\nu) = 4\pi d_L^2 I(\nu) = \frac{8}{\pi}\cos i \int_{r_{\text{in}}}^{r_{\text{ex}}} \int_0^{2\pi} \frac{\nu_e r \, d\phi \, dr}{\exp(\nu_e/T) - 1} \tag{15}$$

Here, d_L is the distance between an observer and the source, and $I(\nu)$ is the Planck distribution function. Generally, the inner and outer edges of accretion disks are chosen from the ISCO radius up to infinity. There is ν_e defined as the emitted frequency given by the redshift factor z as $\nu_e = \nu(1+z)$. The redshift factor z can be written down:

$$1 + z = \frac{1 + \Omega r \sin\phi \sin i}{\sqrt{-g_{tt} - 2\Omega g_{t\phi} - \Omega^2 g_{\phi\phi}}}. \tag{16}$$

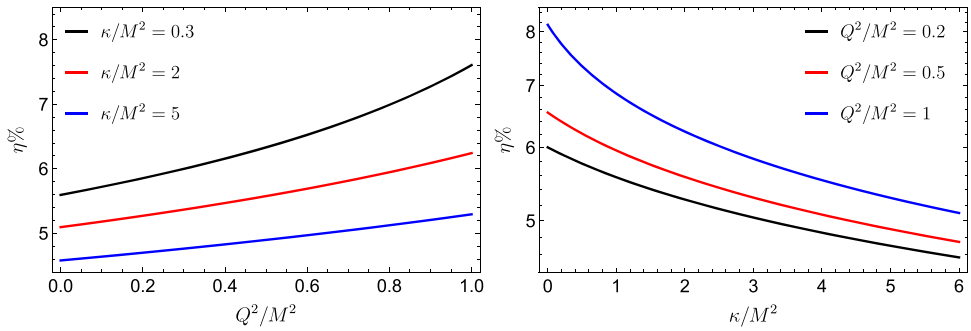

Fig. 7 The radiation efficiency of the accretion disk around the black hole

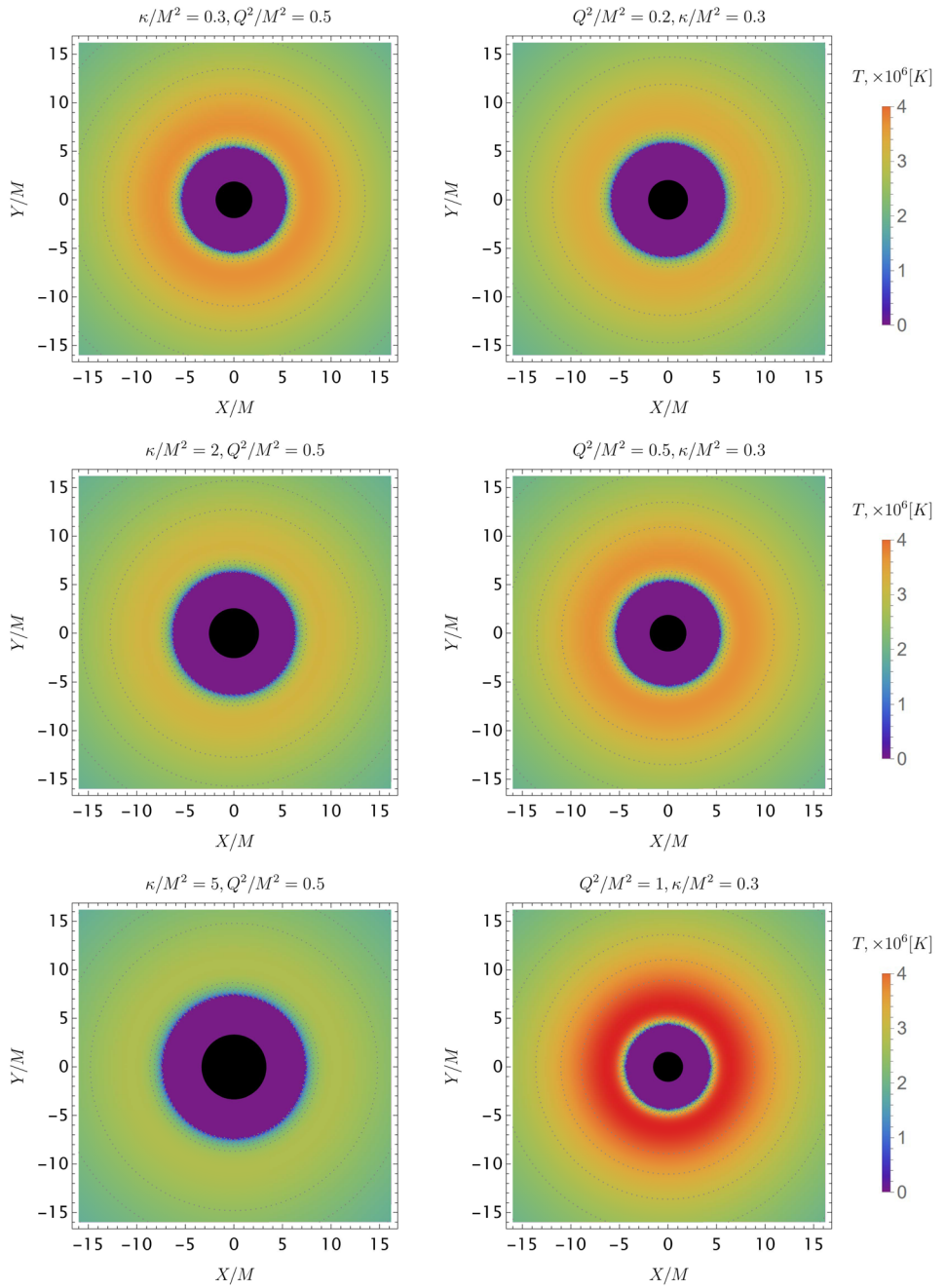

Fig. 8 Temperature profiles represented as density plots at various positions for different values of the parameter

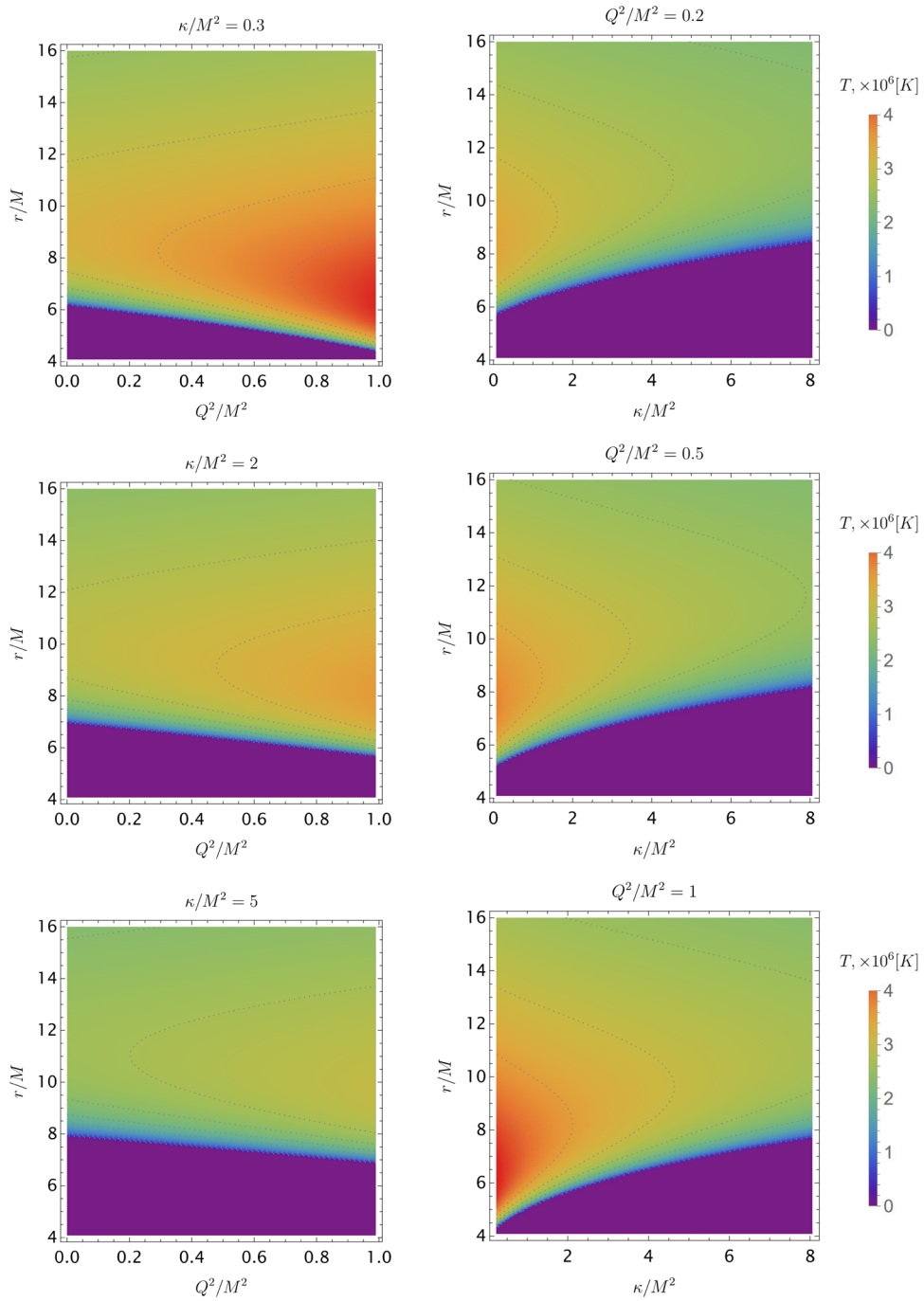

Fig. 9 Temperature profiles represented as density plots for various values of radial distance and spacetime parameters

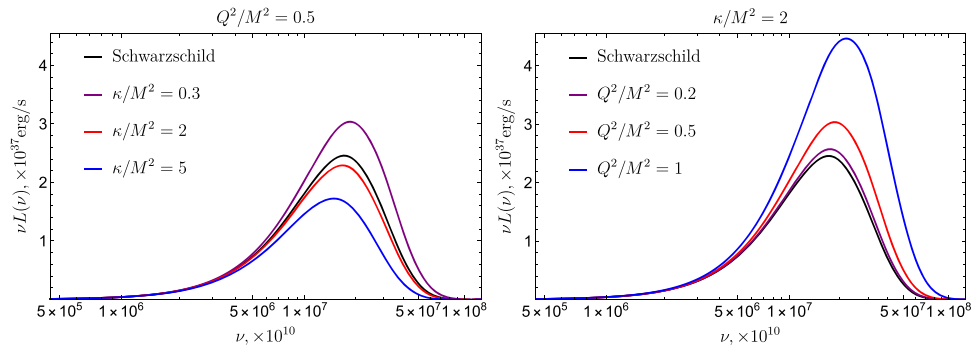

Fig. 10 The spectra of the accretion disk around the black hole with a nonzero geometric charge are presented

Finally, we examine the spectrum of the black holes, shown in Fig. 10. Up to frequencies of about $\nu \approx 3 \times 10^6$ Hz, the parameters κ and the geometric charge Q have an almost negligible effect on the profile. Beyond this point, however, their influence becomes significant, and the luminosity eventually vanishes around $\nu \approx 10^{18}$ Hz. The spectrum attains its maximum luminosity near $\nu \approx 2 \times 10^{17}$ Hz, with the exact peak occurring slightly below or above this value depending on the specific values of κ and Q. In particular, smaller values of Q combined with larger values of κ shift the peak toward lower frequencies, while larger Q and smaller κ shift it toward higher frequencies.

5 Conclusion

Understanding black hole accretion disks in alternative gravity theories remains crucial for testing GR. Beyond Einstein's GR, modified theories, such as our focus here, EGB gravity, offer new insights. In this work, we investigated how the EGB gravity parameters, κ and Q, influence the spacetime geometry, orbital dynamics, and radiative properties of accretion disks around the EGB black hole. We began by analyzing the spacetime metric and showed that, in appropriate limits, the solution reduces to well-known cases such as the Reissner–Nordström and Schwarzschild spacetimes. Notably, the geometric charge Q, which originates from the spacetime structure rather than matter fields, plays a central role in modifying black hole properties.

We showed that both Q and κ significantly influenced key gravitational characteristics such as the event horizon radius, the ISCO radius, and the radiation efficiency of the accretion disk. Although the geometric charge tends to shrink the event horizon and lower the ISCO radius, enhancing radiation efficiency, larger values of the GB coupling generally expand the horizon and move stable orbits outward, reducing efficiency. We have shown that the combined influence of κ and Q can shift the ISCO radius up to $8.62M$.

Through the Novikov–Thorne thin disk model, we computed flux and temperature profiles, revealing that the electromagnetic emissions from the accretion disk are highly sensitive to the interplay between Q and κ. Furthermore, we demonstrated that these parameters can mimic the behavior of rotating Kerr black hole, effectively reproducing spin-like effects even in the absence of rotation. We demonstrated that κ and Q can mimic Kerr spin effects up to $a/M \approx 0.866$. The spectral analysis confirmed that variations in Q and κ lead to observable shifts in peak luminosity frequencies, offering a potential avenue to distinguish this class of modified gravity black holes from standard solutions via high-energy astrophysical observations.

Overall, our findings suggest that geometric charge and GB corrections could leave detectable imprints on accretion disk dynamics and radiation, potentially serving as observational signatures of beyond GR gravitational physics. Future studies may focus on extending this analysis to rotating solutions, dynamical spacetimes, and observational data fitting to further constrain these parameters in astrophysical contexts.

Funding No funding.

Data Availability Statement This manuscript has no associated data. [Authors' comment: Data sharing not applicable to this article as no datasets were generated or analysed during the current study.]

Code Availability Statement Code/software will be made available on reasonable request. [Authors' comment: The code/software generated during and/or analysed during the current study is available from the corresponding author on reasonable request.]

Funded by SCOAP[3].

References

1. B.P. Abbott et al., Phys. Rev. Lett. **116**, 061102 (2016). https://doi.org/10.1103/PhysRevLett.116.061102
2. K. Akiyama et al., Astrophys. J. Lett. **930**, L12 (2022). https://doi.org/10.3847/2041-8213/ac6674
3. N. Pinto-Neto, E.S. Santini, Phys. Lett. A **315**, 36 (2003). https://doi.org/10.48550/arXiv.gr-qc/0302112
4. V. Chirde, S. Shekh, J. Astrophys. Astron. **39**, 56 (2018). https://doi.org/10.1007/s12036-018-9555-0
5. C. Lanczos, Ann. Math. **39**, 842 (1938). https://doi.org/10.2307/1968467
6. D. Lovelock, J. Math. Phys. **12**, 498 (1971). https://doi.org/10.1063/1.1665613
7. D. Lovelock, J. Math. Phys. **13**, 874 (1972). https://doi.org/10.1063/1.1666069
8. M. Ostrogradsky, Mémoires de l'Académie Impériale des Sciences de Saint-Pétersbourg **4**, 385 (1850)
9. D. Glavan, C. Lin, Phys. Rev. Lett. **124**, 081301 (2020). https://doi.org/10.1103/PhysRevLett.124.081301
10. P.G.S. Fernandes, P. Carrilho, T. Clifton, D.J. Mulryne, Class. Quantum Gravity **39**, 063001 (2022). https://doi.org/10.1088/1361-6382/ac500a
11. S.W. Hawking, Commun. Math. Phys. **25**, 152 (1972). https://doi.org/10.1007/BF01877517
12. T. Nakamura, K. Oohara, Y. Kojima, Prog. Theor. Phys. Suppl. **90**, 1 (1997). https://doi.org/10.1143/PTPS.90.1
13. J.P.S. Lemos, Phys. Lett. B **353**, 46 (1995). https://doi.org/10.1016/0370-2693(95)00533-Q
14. M. Dafermos, Commun. Pure Appl. Math. **58**, 445 (2005). https://doi.org/10.1002/cpa.20071

15. B. Toshmatov, Z. Stuchlík, J. Schee, B. Ahmedov, Phys. Rev. D **97**, 084058 (2018). https://doi.org/10.1103/PhysRevD.97.084058
16. S.G. Ghosh, R.K. Walia, Ann. Phys. **434**, 168619 (2021). https://doi.org/10.1016/j.aop.2021.168619
17. J.-Z. Yang, S. Shahidi, T. Harko, Phys. Dark Universe **31**, 100756 (2021). https://doi.org/10.1016/j.dark.2020.100756
18. S.G. Ghosh, M. Afrin, Eur. Phys. J. C **83**, 1108 (2023). https://doi.org/10.1140/epjc/s10052-023-12306-z
19. S.G. Ghosh, R. Kumar, Class. Quantum Gravity **37**, 245008 (2020). https://doi.org/10.1088/1361-6382/abc134
20. S.W. Wei, Y.X. Liu, Eur. Phys. J. Plus **136**, 436 (2021). https://doi.org/10.1140/epjp/s13360-021-01398-9
21. C. Sahabandu, P. Suranyi, C. Vaz, L.C.R. Wijewardhana, Phys. Rev. D **73**, 044009 (2006). https://doi.org/10.1103/PhysRevD.73.044009
22. X.X. Zeng, H.Q. Zhang, H. Zhang, Eur. Phys. J. C **80**, 872 (2020). https://doi.org/10.1140/epjc/s10052-020-08449-y
23. L. Pierini, L. Gualtieri, Phys. Rev. D **103**, 124017 (2021). https://doi.org/10.1103/PhysRevD.103.124017
24. R.A. Konoplya, A.F. Zinhailo, Eur. Phys. J. C **80**, 1049 (2020). https://doi.org/10.1140/epjc/s10052-020-08639-8
25. M.A. Abramowicz, P.C. Fragile, Living Rev. Relativ. **16**, 1 (2013). https://doi.org/10.12942/lrr-2013-1
26. B. Narzilloev, J. Rayimbaev, A. Abdujabbarov, B. Ahmedov, Galaxies **9**, 63 (2021). https://doi.org/10.3390/galaxies9030063
27. B. Narzilloev, B. Ahmedov, Symmetry **14**, 1765 (2022). https://doi.org/10.3390/sym14091765
28. B. Narzilloev, B. Ahmedov, New Astron. **98**, 101922 (2023). https://doi.org/10.1016/j.newast.2022.101922
29. B. Narzilloev, A. Abdujabbarov, A. Hakimov, Int. J. Mod. Phys. A **37**, 2250144 (2022). https://doi.org/10.1142/S0217751X22501445
30. B. Narzilloev, B. Ahmedov, Symmetry **15**, 293 (2023). https://doi.org/10.3390/sym15020293
31. T. Mirzaev, S. Li, B. Narzilloev, I. Hussain, A. Abdujabbarov, B. Ahmedov, Eur. Phys. J. Plus **138**, 47 (2023). https://doi.org/10.1140/epjp/s13360-023-03647-5
32. B. Narzilloev, B. Ahmedov, Int. J. Mod. Phys. A **38**, 2350026 (2023). https://doi.org/10.1142/S0217751X23500262
33. A. Davlataliev, B. Narzilloev, I. Hussain, A. Abdujabbarov, B. Ahmedov, Phys. Dark Universe **46**, 101569 (2024). https://doi.org/10.1016/j.dark.2024.101569
34. U. Uktamov, B. Narzilloev, I. Hussain, A. Abdujabbarov, B. Ahmedov, Phys. Dark Universe **49**, 102022 (2025). https://doi.org/10.1016/j.dark.2025.102022
35. M.A. Abramowicz, P.C. Fragile, Living Rev. Relativ. **16**, 1 (2013). https://doi.org/10.12942/lrr-2013-1
36. A. Sadowski, J.-P. Lasota, M.A. Abramowicz, R. Narayan, Mon. Not. R. Astron. Soc. **456**, 3915 (2016). https://doi.org/10.1093/mnras/stv2854
37. J. Bagchi, M. Vivek, V. Vikram, A. Hota, K.G. Biju, S.K. Sirothia, R. Srianand, Gopal-Krishna, J. Jacob, Astrophys. J. **788**, 174 (2014). https://doi.org/10.1088/0004-637X/788/2/174
38. J.S. Spilker, J.B. Champagne, X. Fan, S. Fujimoto, P.P. van der Werf, J. Yang, M. Yue, Astrophys. J. **982**, 72 (2025). https://doi.org/10.3847/1538-4357/adab15
39. P. Mészáros, D.B. Fox, C. Hanna, K. Murase, Nat. Rev. Phys. **1**, 585 (2019). https://doi.org/10.1038/s42254-019-0101-z
40. M. Bousder, K. El Bourakadi, M. Bennai, Phys. Dark Universe **32**, 100839 (2021). https://doi.org/10.1016/j.dark.2021.100839
41. R. Narayan, S. Kato, F. Honma, Astrophys. J. **476**, 49 (1997)
42. I.D. Novikov, K.S. Thorne, in *Black Holes*. ed. by C. De Witt, B. De Witt (Gordon and Breach, New York, 1973), p.343
43. S. Sengupta, J. Cosmol. Astropart. Phys. **2022**, 020 (2022). https://doi.org/10.1088/1475-7516/2022/02/020
44. S. Gera, P.D. Roy, arXiv:2308.11719 (2023)